



Synchronization of branching chain of dynamical systems

Michele Baia ^{a,b}, Franco Bagnoli ^{a,b}, Tommaso Matteuzzi ^a, Arkady Pikovsky ^c

^a Department of Physics and Astronomy and CSDC, University of Florence, G. Sansone, 1, Sesto Fiorentino, 50019, Italy

^b INFN, Sect. Florence, G. Sansone, 1, Sesto Fiorentino, 50019, Italy

^c Institute of Physics and Astronomy, University of Potsdam, Karl-Liebknecht-Str. 24/25, Potsdam-Golm, 14476, Germany

ARTICLE INFO

Communicated by Dmitry Pelinovsky

Keywords:

Master–slave (parent–child) synchronization
Child–child synchronization
Branching chain
Logistic map
Machine precision synchronization
Spatio-temporal chaotic maps
Instability due to numerical precision errors

ABSTRACT

We investigate the synchronization dynamics in a chain of coupled chaotic maps organized in a single-parent family tree, whose properties can be captured considering each parent node connected to two children, one of which also serves as the parent for the subsequent node. Our analysis focuses on two distinct synchronization behaviors: parent–child synchronization, defined by the vanishing distance between successive nodes along the chain, and sibling synchronization, corresponding to the convergence of the states of two child nodes. Our findings reveal significant differences in these two type of synchronization mechanisms, which are closely associated with the probability distribution of the state of parent node. Theoretical analysis and simulations with the logistic map support our findings. We further investigate numerical aspects of the implementation corresponding to cases for which the simulated regimes differ from the theoretically predicted one due to computational finite accuracy. We perform a detailed study on how instabilities are numerically suppressed or amplified along the chain. In some cases, a properly adjusted computational scheme can solve this problem.

1. Introduction

Complete synchronization of chaotic systems has been first studied for two identical coupled units, whose states can become equal if the coupling is strong enough to suppress the chaotic instability [1,2]. This type of phenomenon is widely studied in the literature, from discrete maps to low dimensional continuous systems or defined on networks and hypergraphs [3–5], and with different application, from cryptography [6] to data assimilation [7]. In spatially extended systems, such as coupled map lattices [8], synchronization implies spatial homogeneity across the system. For such systems, one typically considers a local symmetric spatial coupling, though asymmetric forms have also been explored [9].

A notable example of asymmetric coupling is unidirectional or parent–child (alternatively referred to as master–slave) coupling of identical systems. Here, part of the signal from the parent system is injected into the child [10], but there is no action in the opposite direction. The synchronization threshold is related to the chaotic properties of the uncoupled system. If the coupling strength exceeds a certain threshold, the states of the two systems become identical, provided that their parameters are the same. In many setups of this type of coupling configurations, there exists a relationship between the maximum Lyapunov exponent of the parent (the unperturbed system) and the critical coupling strength needed to achieve synchronization.

Furthermore, the same parent signal can be directed to multiple child systems, enabling studies of mutual synchronization among these “children”. Here, the parent signal can be seen as a common noise source, albeit correlated with the states of children. Such a situation is relevant for the brain dynamics, where remote synchronization can occur when neurons connected to a hub node, under appropriate coupling conditions, synchronize with each other [11].

Intriguingly, noise-induced synchronization has been widely studied [9,12–14], yielding unexpected findings, such as the potential of randomness to promote synchronization even for chaotic conditions [15]. Recent researches expanded these foundational theories, focusing on synchronization generalizations. Notable advances include the study of phase synchronization [16] and generalized synchronization [17], these phenomena occur even with parameter mismatches.

It is possible to extend the master–slave synchronization approach to spatio-temporal chaos, for instance coupled map lattices [18], spatio-temporal chaotic systems [19], and cellular automata [20].— These efforts aim to link synchronization behaviors to universal classes such as directed percolation and the KPZ class [21–23].

This work addresses the problem of parent–child synchronization in a unidirectional network structured as a Cayley tree (see Fig. 1). The tree is organized in layers; the units at layer i drive unidirectionally units of layer $i + 1$, $i = 0, 1, 2, \dots$. The symmetry of units within a layer

* Corresponding author at: Department of Physics and Astronomy and CSDC, University of Florence, G. Sansone, 1, Sesto Fiorentino, 50019, Italy.

E-mail addresses: michele.baia@unifi.it (M. Baia), franco.bagnoli@unifi.it (F. Bagnoli), tommaso.matteuzzi@unifi.it (T. Matteuzzi), pikovsky@uni-potsdam.de (A. Pikovsky).

<https://doi.org/10.1016/j.physd.2025.134664>

Received 26 November 2024; Received in revised form 3 March 2025; Accepted 29 March 2025

Available online 12 April 2025

0167-2789/© 2025 The Authors. Published by Elsevier B.V. This is an open access article under the CC BY-NC-ND license (<http://creativecommons.org/licenses/by-nc-nd/4.0/>).

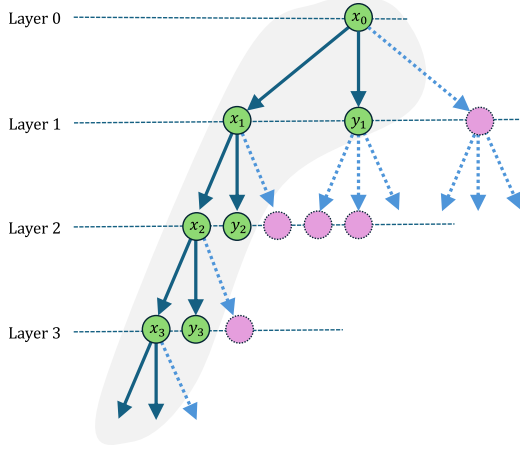


Fig. 1. The selection of the branching chain. We start with a full Cayley tree (with levels denoted as “layers”) with unidirectional coupling. For symmetry reasons, the behavior of all nodes in the same layer is the same, so we consider only two nodes (“siblings”) for each layer except for the top one (layer 0).

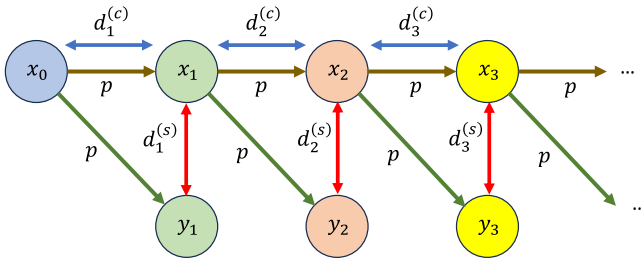


Fig. 2. Branching chain scheme. The sub-index i denotes layers. The arrow marked p denotes the one-directional coupling (see Eq. (2)). The two-directional arrows denotes distances. Node labeled x_0 is the first parent. It has two “children”, x_1 and y_1 , and we measure the distance $d_1^{(c)} = |x_0 - x_1|$ between the parent and one of its children, and $d_1^{(s)} = |x_1 - y_1|$ between the two “siblings”. This scheme repeats itself at each layer i .

allows us to assume equivalent behavior across nodes at the same layer, therefore we simplify the model by considering only two nodes (or “siblings”) per layer (excluding the root layer $i = 0$). The motivation of this choice is that many generic networks with sparse random links among nodes locally have the structure of a tree. We assume that a node acts as a pacemaker, sending signal to connected nodes, which then forward it to connected nodes and so on. This is also the structure of a feed-forward network starting from a single node. This simplification reduces our study to a branching chain of chaotic maps, illustrated in Fig. 2. Our analysis focuses not only on the interaction between a parent and its child but also on the comparison of the states of siblings sharing a parent signal, assessing how siblings synchronize with each other and with their parent. Specifically, we study a chain of logistic maps as an illustrative case, which reveals distinctive synchronization behaviors. Synchronization of coupled logistic maps of a Cayley tree has been explored in literature, using different coupling configuration and different purposes. In Refs. [24–26] the pattern formation and the synchronization states were analyzed when the nodes are coupled with a reaction–diffusion coupling. In Ref. [27] instead, the coupling was asymmetric but non completely oriented, and the main results concerned the stability of synchronous state, related to the spectrum of the coupling matrix.

In Section 2, we outline the model general structure, followed by a specific investigation of a logistic map chain in Section 3. This work is an extension of the preliminarily results presented in [28]: we will demonstrate that unexpected phenomena arise, particularly that siblings can achieve synchronization at much smaller coupling

strengths than those required for parent–child synchronization. This behavior is linked to synchronization driven by common noise [14,15,29]. Moreover, we highlight the impact of the computational method on simulating such chaotic coupled systems, noting that certain numerical schemes can introduce spurious dynamics, influenced by both the intrinsic chaotic nature of the system and the limitations of computational number representation.

2. The branching chain model

We consider one-dimensional maps $x(t+1) = f(x(t))$, where the variable $x \in [0, 1]$ evolves in discrete time steps, indexed by the time index t . In the following, we shall indicate by $x \equiv x(t)$ and $x' \equiv x(t+1)$.

Let us consider a branching chain scheme (Fig. 2) in which the first map is an autonomous “pacemaker”

$$x'_0 = f(x_0), \quad (1)$$

and all other maps are driven by their “parent map”

$$\begin{aligned} x'_i &= (1-p)f(x_i) + pf(x_{i-1}), \\ y'_i &= (1-p)f(y_i) + pf(x_{i-1}). \end{aligned} \quad (2)$$

Here the parameter $p \in [0, 1]$ defines the strength of the coupling and the lower index i denotes the layer number. This setup can be seen as the minimal sampling in a full Cayley tree, see Fig. 1, where the first node x_0 is the root and for each subsequent layer $i > 0$ only the two x_i and y_i nodes are selected.

Before proceeding, let us define the standard Lyapunov exponent for the maps (1),(2). The linearized dynamics of a small perturbation $\delta x_i(t)$ around a trajectory $x_i(t)$ is governed by

$$\delta x'_i = \begin{cases} \frac{df}{dx}(x_i)\delta x_i & \text{for } i = 0, \\ (1-p)\frac{df}{dx}(x_i)\delta x_i & \text{for } i \geq 1. \end{cases}$$

Accordingly, the Lyapunov exponents Λ_i are defined as the averaged growth rates of the logarithms of typical perturbations [30]:

$$\begin{aligned} \Lambda_0 &= \left\langle \ln \left| \frac{df}{dx}(x_0) \right| \right\rangle \equiv \lambda_0, \\ \Lambda_{i>0} &= \ln(1-p) + \left\langle \ln \left| \frac{df}{dx}(x_i) \right| \right\rangle \equiv \ln(1-p) + \lambda_i, \end{aligned} \quad (3)$$

where for convenience of further analysis we introduced a notation

$$\lambda_i = \left\langle \ln \left| \frac{df}{dx}(x_i) \right| \right\rangle, \quad i = 0, 1, 2, \dots$$

For each layer, the two siblings x_i and y_i are guided by the same parent x_{i-1} in the spirit of the Pecora–Carroll scheme [2,7,10] (when applied to maps). Such a setup is usual in the theory of generalized synchronization, where a “replica” of a driven element is introduced [17].

This configuration allows us to define two types of synchronization:

- the *synchronization within a layer*, when $y_i(t) = x_i(t)$,
- the *synchronization across the layers*, which means that $x_i(t) = x_{i-1}(t) = \dots = x_0(t)$ for all t .

The synchronization within a layer can be characterized by computing the average of the difference $d_i^{(s)} = |x_i - y_i|$:

$$s_i = \langle d_i^{(s)} \rangle = \langle |x_i - y_i| \rangle = \frac{1}{T} \sum_{t=\tau}^{\tau+T} |x_i(t) - y_i(t)|,$$

where τ is a transient interval. When s_i vanishes, it means that both “siblings” x_i and y_i follow the common drive x_{i-1} in the same way.

Synchronization across the layers, on the other hand, can be characterized by calculating the average in time difference $d_i^{(c)} = |x_i - x_{i-1}|$:

$$c_i = \langle d_i^{(c)} \rangle = \langle |x_i - x_{i-1}| \rangle = \frac{1}{T} \sum_{t=\tau}^{\tau+T} |x_i(t) - x_{i-1}(t)|,$$

checking if this quantity vanishes.

A transition to complete synchronization across all layers is expected at a critical value of the coupling parameter p , as $c_i > 0$ when $p = 0$ and $c_i = 0$ when $p = 1$. The critical value for the synchronization across all the layers, independent of the index layer i , is designated as $p^{(c)}$.

Since all nodes in the same layer experience the same dynamic, when there is synchronization between layers the elements within each layer are also fully synchronized. However, as we will demonstrate, the reverse is not necessarily true: synchronization can occur within individual layers at coupling values below the threshold $p^{(c)}$. Furthermore, synchronization within certain layers can be achieved even as layers with higher indices i remain desynchronized. This behavior for the logistic map is illustrated in Fig. 4.

Following standard approaches in complete synchronization theory, a criterion can be established by analyzing the behavior of small perturbations near the synchronized state [9]. In order to do that, let us consider the synchronization of the first child x_1 with the parent x_0 . Near the synchronization transition across the layers, $c_1 \simeq 0$, we can write $x_1(t) = x_0(t) + \delta x_1(t)$ and, using Eq. (2), we obtain:

$$\delta x_1' = (1-p) \frac{df}{dx}(x_0) \delta x_1.$$

Thus, the exponential growth rate of the perturbations to the complete synchrony is

$$\lambda_1^{(c)} = \ln(1-p) + \left\langle \ln \left| \frac{df}{dx}(x_0) \right| \right\rangle = \ln(1-p) + \lambda_0, \quad (4)$$

where $\lambda_0 = \Lambda_0 = \left\langle \ln \left| \frac{df}{dx}(x_0) \right| \right\rangle$ is the Lyapunov exponent of the driving map at level 0. From the above expression, the theoretical estimate of the critical value of the coupling can be easily obtained:

$$p^{(c)} = 1 - \exp(-\lambda_0). \quad (5)$$

Assuming that the parent–children synchronization starts from the top layers (first x_1 with x_0 , then x_2 with x_1 , etc.), this relation is valid for the first non-synchronized layer, and thus in principle all layers should experience synchronization transition at the same value of $p^{(c)}$.

We can repeat the analogous calculations for the siblings, computing the evolution of the divergence δy_i of the trajectory as a function of the dynamic variable x of the first sibling

$$\delta y_i' = y_i' - x_i' = (1-p) \left(\frac{df}{dx}(x_i) \right) (y_i - x_i) = (1-p) \left(\frac{df}{dx}(x_i) \right) \delta y_i.$$

The exponential growth rate of the perturbation can be written as

$$\lambda_i^{(s)} = \ln(1-p) + \left\langle \ln \left| \frac{df}{dx}(x_i) \right| \right\rangle = \ln(1-p) + \lambda_i, \quad (6)$$

and, therefore

$$p_i^{(s)} = 1 - \exp(-\lambda_i). \quad (7)$$

Note that, since x_i and x_0 are not synchronized in general, the quantity $\lambda_i = \left\langle \ln \left| \frac{df}{dx}(x_i) \right| \right\rangle$ defined above is not the Lyapunov exponent of the uncoupled map, but depends on the local dynamics of x_i . As above, this value can be calculated from the probability density distribution $P_i(x)$ of the variable x_i ,

$$\lambda_i = \int_0^1 \ln \left(\left| \frac{df}{dx}(x) \right| \right) P_i(x) dx. \quad (8)$$

3. Chain of logistic maps

Below we consider a chain of logistic maps at the Ulam point defined by the recurrence equation

$$x' = 4x(1-x). \quad (9)$$

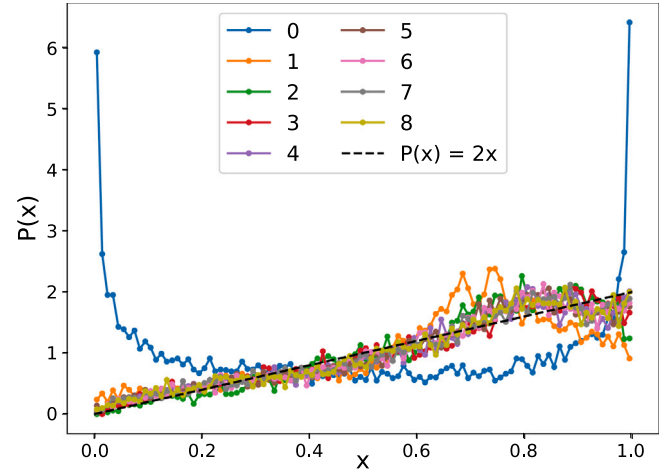


Fig. 3. Probability density distribution $P_i(x)$ of maps along the chain for $p = 0.32$, and the linear approximation (straight black dashed line). $P_0(x)$ is the probability density distribution of the unperturbed logistic map. For $i \geq 1$ the probability distribution is influenced by the dynamic of the node in the previous layer, thus $P_i(x) \neq P_0(x)$.

The stationary probability density distribution of the state variable x is $P_0(x) = \left(\pi \sqrt{x(1-x)} \right)^{-1}$, see Fig. 3. The corresponding Lyapunov exponent is

$$\lambda_0 = \int_0^1 \frac{\ln(4|1-2x|)}{\pi \sqrt{x(1-x)}} dx = \ln(2). \quad (10)$$

This yields, according to the general relation (5), $p^{(c)} = \frac{1}{2}$.

3.1. Patterns of synchrony in a small chain

In the absence of the complete synchronization across the layers, i.e., for $p < p^{(c)}$, the regimes at $i > 0$ are different from that of Eq. (9) and the form of the probability density varies with the layer number i . Fig. 3 indicates that for large i , the distributions for different i become nearly equal and are well approximated by $P(x) = 2x$. This probability shape is similar to the one reported in Fig. 4 of Ref. [27], obtained for asymmetrically coupled logistic maps on a Cayley tree. Inserting this approximation in the relation (8), we get $\lambda_i = \ln(4) - 1 \approx 0.386$. The corresponding approximate value of the critical coupling according to Eq. (7) is $p_i^{(s)} \approx 0.32$ in good agreement with Fig. 4(b).

In Figs. 4 and 5 we show the results of our simulations with a limited number of nodes with logistic maps: we plot the average distances c_i (Fig. 4(a)) and s_i (Fig. 4(b)) for the first 10 layers of the system. In Fig. 5 we show the computed sibling Lyapunov exponents, $\lambda_i^{(s)}$, and we also plot the first computed parent–child Lyapunov exponent $\lambda_1^{(c)}$ (labeled 0 in legend). Note that for $p > p^{(c)}$ all nodes are synchronized, so the Lyapunov exponent follows the same behavior for all nodes.

We can notice that the transition to parent–children synchronization across the layers occurs for all layers around the estimated value (Eq. (5)) $p^{(c)} \simeq 0.5$, although with quite a different behavior near the transition threshold. Synchronization within a layer starts at a value of $p_i^{(s)} \simeq 0.32 < p^{(c)}$.

3.2. Synchronization window with a chessboard pattern

There is also a synchronization-within-a-layer window near $p = 0.18$, which can be explained as follows. A detailed visual inspection (Fig. 6) reveals that here a chessboard-like spatio-temporal pattern close to having period 2 both in space and time is observed. Let us assume that such a pattern is superstable, i.e. it contains the point $x = 1/2$ at which $f'(x) = 0$. Such a pattern has a form $x_{2m+1}(2k+1) =$

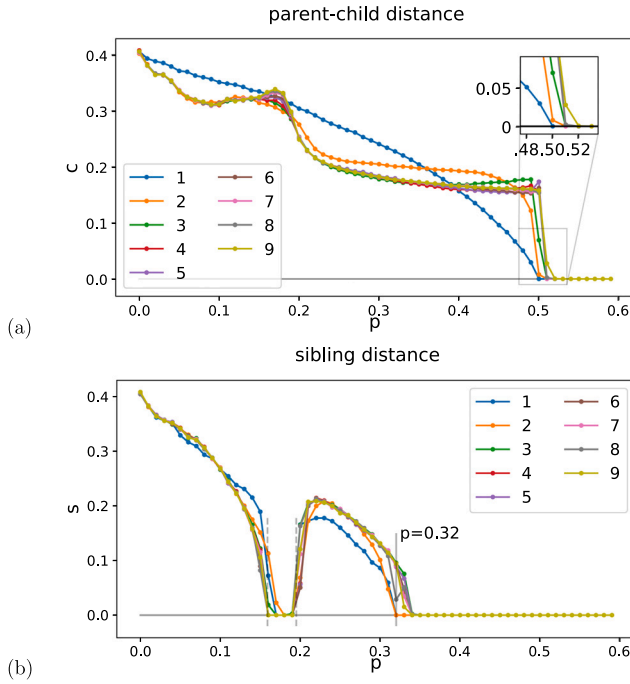


Fig. 4. The distances between parent and child (a) and between the two siblings (b) for the first 10 layers of the logistic chain (total length 11 layers); $T = 10^4$, $\tau = 10^5$.

$x_{2m}(2k) = \frac{1}{2}$, $x_{2m+1}(2k) = x_{2m}(2k + 1) = X$ with some unknown X . It is a solution of the logistic chain if

$$\frac{1}{2} = pf\left(\frac{1}{2}\right) + (1-p)f(X), \quad X = pf(X) + (1-p)f\left(\frac{1}{2}\right).$$

This system of equations has a solution

$$X = \frac{3 + \sqrt{17}}{8}, \quad p = \frac{5 - \sqrt{17}}{9 - \sqrt{17}} \approx 0.1798.$$

One can expect that around this superstable value of the parameter, $0.16 \lesssim p \lesssim 0.2$ the pattern will still be stable. However, a perfect period-2 pattern will be only observed for a particular period-2 trajectory at site $i = 0$. For a generic chaotic driving $x_0(t)$, one, first, starts to observe this pattern for large enough i , and second, this pattern is not perfect. At large distances from edge $i = 0$, one observes long patches of the period-2 behavior intermingled with defects (Fig. 6); the number of defects decreases with i . This explains why only at large i the transversal Lyapunov exponent for the stability within a layer becomes negative (cf. Fig. 5).

There is, however, a visible contradiction between the transversal exponent $\lambda_1^{(c)}$ (Fig. 5) and the observed distance s_i (Fig. 4) in the region $p \approx 0.18$. Indeed, even for small i where $\lambda_1^{(c)} > 0$, synchronization within a layer is observed.

This ‘‘anomalous’’ synchronization can be understood as a result of finite-precision effects of numerical simulations (cf. Ref. [31]). Even when the transversal Lyapunov exponent is positive, fluctuations in the distance between systems x_i and y_i can reduce this distance to such a small value that the computer representations of the states coincide. Afterward, the states remain identical, despite the presence of transversal instabilities.

To verify this hypothesis, one can rerun the numerical simulations with increased precision ϵ , for instance, increasing from $\epsilon = 32$ bit up to $\epsilon = 512$ bit, and compare the differences $|x_i - y_i|$ with those obtained in previous simulations using 64-bit precision.

In Fig. 7(a), we present the siblings-distance $s_1 = \langle |x_1 - y_1| \rangle$, computed at different levels of ϵ . As shown, increasing the precision

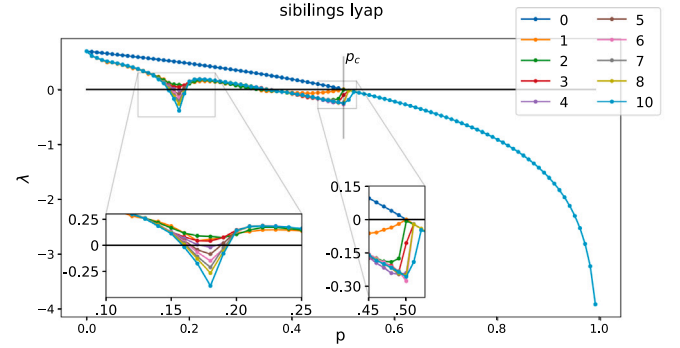


Fig. 5. The computed Lyapunov exponent $\lambda_1^{(c)}$ (0 in legend) and the Lyapunov exponent $\lambda_i^{(s)}$ of the chain (total length 11 layers); $T = 10^4$, $\tau = 10^5$.

leads to a change in the width of the synchronized window, which vanishes for $\epsilon > 128$ bit.

Additionally, in Fig. 7(b), we present an example of the behavior of the sibling distance $d_1^{(s)}(t) = |x_1(t) - y_1(t)|$ at the first node for $p = 0.18$. Specifically, we compare this distance at low precision ($\epsilon = 64$) with that at high precision ($\epsilon = 256$). It is evident that higher machine precision leads to more accurate numerical representations, resulting in a minimum distance between the two nodes on the order of 10^{-20} . At lower precision, synchronization is driven by approximation truncation: at the given coupling parameter, the distance eventually falls below machine precision, becoming numerically zero. A statistical analysis, based on 1000 simulations, shows that the distance between the sibling in the first layer, s_1 , for coupling values $p = 0.18$ with a precision of 64-bit we have probability 1 of having synchronization, with a precision of 256-bit this drops to the 0.2%. Intriguing is the case at 128 bits, where we have a 50% probability that the distance between siblings in the first layer drops below the machine precision and, therefore, of having synchronization. If we analyze the distance for deeper layers, we observe that even for greater numerical precisions, the distance ends up below the machine threshold, creating fictitious synchronized states. For example, for 256-bit precisions, from the fourth layer, the probability of having synchronized sibling states returns to 100% (compare Fig. 8 left column for 64-bit values). We expect that this phenomenon will disappear only with infinite numerical precision.

3.3. Importance of the numerical implementation for large chains

Before describing the results obtained for the deep system, e.g., with a number of layer $\gg 10$, let us consider how the coupling scheme can be rewritten in two mathematically equivalent formulations, which, however, yield profoundly different computational results when combined with the map of Eq. (9).

Eq. (2) can be computationally implemented using the *direct coupling* scheme, as defined in the mathematical model:

$$\begin{aligned} x'_i &= (1-p)f(x_i) + pf(x_{i-1}); \\ y'_i &= (1-p)f(y_i) + pf(y_{i-1}). \end{aligned} \tag{11}$$

Another possible numerical implementation is a *delta coupling*

$$\begin{aligned} x'_i &= f(x_i) + p(f(x_{i-1}) - f(x_i)); \\ y'_i &= f(y_i) + p(f(y_{i-1}) - f(y_i)), \end{aligned} \tag{12}$$

where first, a difference of the values at two layers is calculated, and then multiplied by p and added to the value at the current layer.

In Fig. 8 we show the results for the distances (parent–child across the layers and siblings within a layer) obtained using the two different computational schemes (Eqs. (11), (12)). As we can see, the behavior of the synchronization state at $p > p^{(c)}$ in this kind of system is strongly

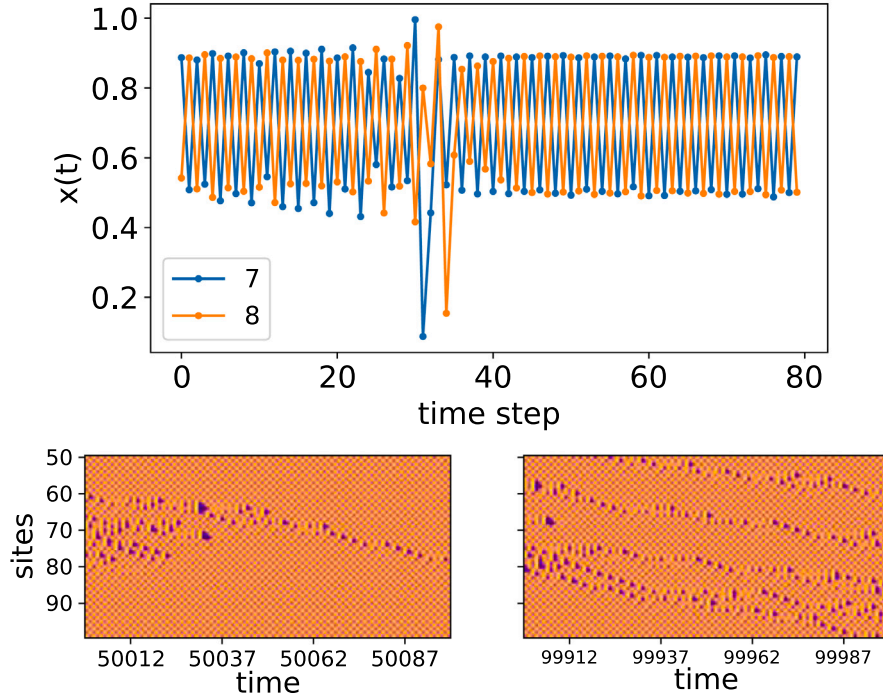


Fig. 6. (Top) Snapshot of the time evolution of maps $x_7(t)$ and $x_8(t)$ for $p = 0.18$ and (bottom) heat map of the time evolution of the nodes in the deeper layers (total length 100 layers). In both cases we show the time evolution for each time step. $T = 10^5$, $\tau = 10^4$.

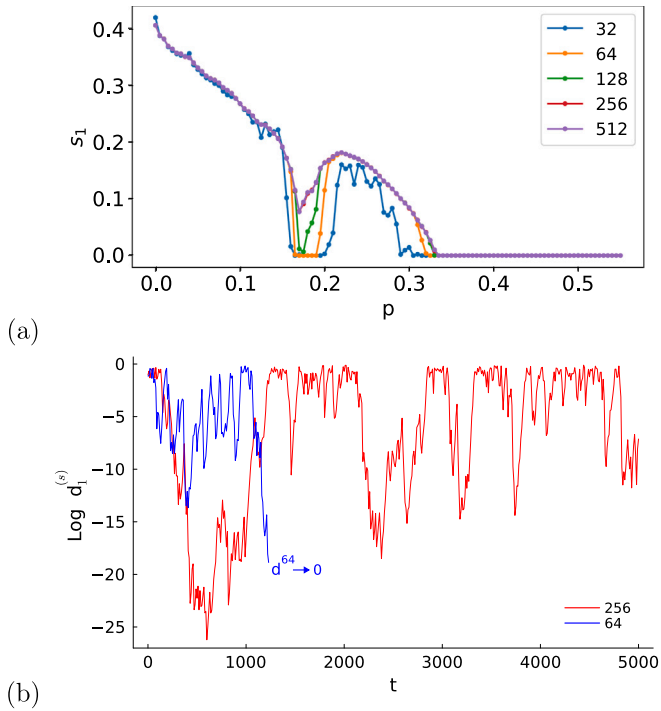


Fig. 7. (a) Siblings distances of the first node (s_1) computed with different machine precision ϵ (values in legend). Only for precision $\epsilon \geq 256$ bit does the synchronization window disappear. Here $T = 10^4$, $\tau = 10^5$. (b) Plot of the time evolution of the siblings distance of the first nodes ($\log_{10} d_1^{(s)}$) computed with $\epsilon = 64$ and $\epsilon = 256$ machine precision at coupling parameter $p = 0.18$. The distance with 64-bit precision may eventually reach values lower than machine precision, creating artificial synchronized states.

influenced by the computational scheme used to implement Eq. (2) for the distance across the layers for deeper nodes (> 10).

In particular, for coupling values greater than the critical value $p^{(c)}$, it is not possible to obtain a completely synchronized state when the simulation is performed with the direct computation scheme.

3.3.1. Boundary sensitivity of the synchronized dynamics

The reason for the sensitivity of the dynamics to the numerical scheme lies in the convective instability of the synchronous dynamics. This effect in coupled map lattices has been discussed in Refs. [32,33] in the context of asymmetrically coupled map lattices, which also includes the unidirectional coupled chain of the present study. Indeed, the usual Lyapunov exponent measures the on-site evolution of a perturbation, while a perturbation can decay on-site but propagate along the chain as a pulse with growing amplitude. To identify such a state, one needs to calculate a velocity-dependent (a.k.a. comoving) Lyapunov exponent $\lambda(v)$ which explores growth rates from a localized in space initial perturbation along the spatial-temporal rays propagating with different velocities v [30,34]. Usual Lyapunov exponent appears in this formalism as $\lambda(0)$, and convective instability happens if $\lambda(0) < 0$ but $\lambda(v) > 0$ for some $v \neq 0$.

The velocity-dependent Lyapunov exponent for an asymmetrically coupled map lattice has been calculated in Ref. [33], in our case

$$\lambda(v) = \ln 2 + (1 - v) \ln \frac{1 - p}{1 - v} + v \ln \frac{p}{v}. \quad (13)$$

One can easily check that, indeed, for $p > 1/2$, the homogeneous synchronous state is convectively unstable.

3.3.2. Propagation of local disturbance in a convectively unstable regime

One experiment where this relation can be checked is to calculate the time to re-synchronization if a local perturbation is added. Assuming the system is in a state of complete synchronization ($p \gtrsim p_c$) we initialize the chain in a synchronized configuration such that $x_i(0) = x_0(0)$. A small perturbation is introduced to the initial condition of the

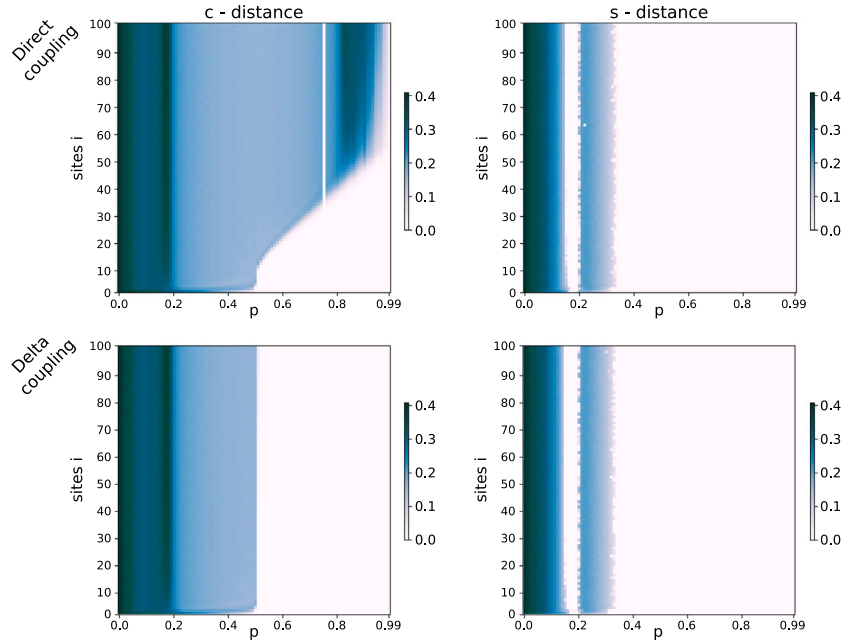


Fig. 8. Heat maps of the parent–child distances (left column) and sibling distances (right column) for a system with 100 layers. In the first row we show the results obtained with the *direct coupling* scheme, Eq. (11), in the second are shown the same plot for the *delta coupling*, Eq. (12).

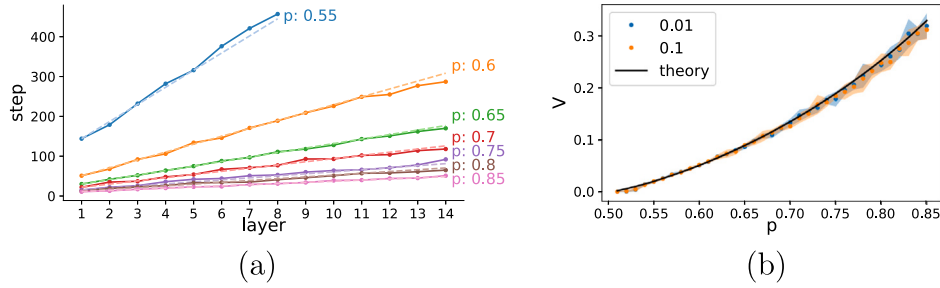


Fig. 9. (a) Number of time steps needed to reabsorb a perturbation of amplitude η from a globally synchronized state. In the dashed line, the linear fit is shown. $T = 10^3$, $\eta = 0.001$. (b) Velocity versus coupling parameter for different initial noise values η (in legend) and, in black line, the theoretical value estimated by solving $\lambda(V) = 0$ in Eq. (13) numerically.

first node $x_0(0) \rightarrow x_0(0) + \eta$. This perturbation spreads along the chain, but eventually, all nodes return to the synchronized state. We analyze the time required for each node to resynchronize, utilizing the *delta coupling* scheme for the computational scheme. In Fig. 9(a), we present, for various coupling values, the number of time steps t needed for the distance $d_i^{(0)}(t) = |x_i(t) - x_0(t)|$ between the first node (x_0) and the i^{th} node to fall below a predefined threshold (set at 10^{-8}) when subjected to a disturbance of intensity $\eta = 0.001$. As observed, the behavior is approximately linear. The slope estimated from the data allows us to define a propagation velocity of the perturbation, or more precisely, a velocity at which the disturbance is reabsorbed along the chain. This velocity approaches zero at the critical threshold $p^{(c)}$, indicating the divergence of the reabsorption times.

The reabsorption velocity V can be determined by finding the velocity at which the velocity-dependent Lyapunov exponent (Eq. (13)) vanishes: $\lambda(V) = 0$. In Fig. 9(b), we compare the simulation results with theoretical predictions (to find V , we found the root of Eq. (13) numerically), showing that this approximation holds well.

3.3.3. Spatial amplification of persistent boundary perturbations

In Section 3.3.2 we considered a single local perturbation at the boundary, while here we look at a persistent perturbation on top of a synchronous state $x_n(t) = X(t)$ at $p > \frac{1}{2}$. A small perturbation $z_n(t) = x_n(t) - X(t)$ evolves in the linear approximation according to

$$z_n(t+1) = f'(X(t))[pz_{n-1}(t) + (1-p)z_n(t)]. \quad (14)$$

Let us consider the *spatial* evolution of the field $z_n(t)$. Namely, we fix the time interval $1 \leq t \leq T$ and set a random homogeneous in time boundary condition $z_0(t)$ (e.g., from a uniform distribution). Then we iterate Eq. (14) in space to find the fields $z_1(t), z_2(t), \dots$. It is convenient, to avoid boundary in time effects, to use periodic boundary conditions in t (i.e. we set $z_n(1) \equiv z_n(T+1)$). The field $z_n(t)$ grows with n , as illustrated in Fig. 10.

The logarithmic scale in Fig. 10 suggests exponential growth of the perturbations in space. This can be quantified with the spatial Lyapunov exponent (see [35] for a growth rate of periodic in time perturbations)

$$\Lambda = \lim_{n \rightarrow \infty} \ln \frac{|z_n(t)|}{|z_0(t)|}. \quad (15)$$

This quantity in dependence on p is shown in Fig. 11 for the logistic map. The spatial Lyapunov exponent defines an effective “boundary layer” close to the left end $i = 0$, within which one can observe synchronization: $\Delta \approx \Lambda^{-1} \ln |\nu_0|$. One can see that this domain grows with parameter p and is minimal close to the synchronization threshold $p \gtrsim \frac{1}{2}$.

3.3.4. Numerical scheme as a source of boundary perturbations

We have observed that the two computational schemes exhibit significantly different results for coupling values greater than the critical value, particularly in the behavior of the deeper layers of the system.

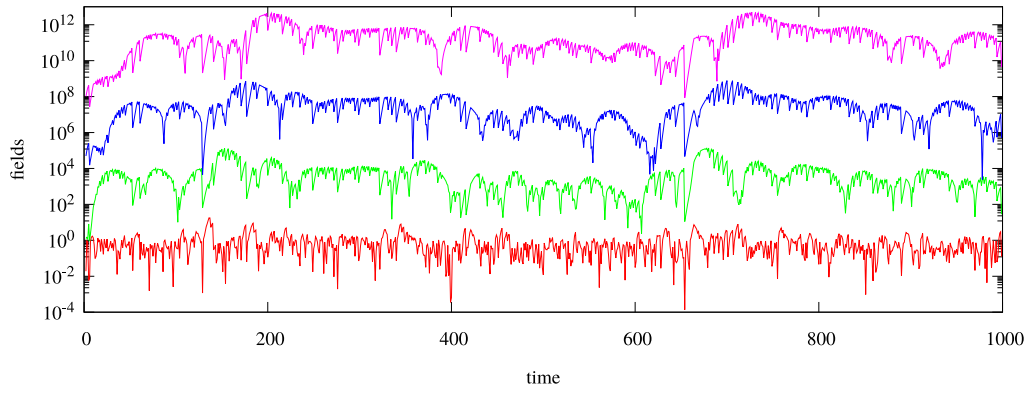


Fig. 10. Evolution in space of the perturbation field $|z_n(t)|$ for $p = 0.6$. Lines show (from bottom to top) $n = 1$ (red), $n = 6$ (green), $n = 11$ (blue) and $n = 16$ (magenta).

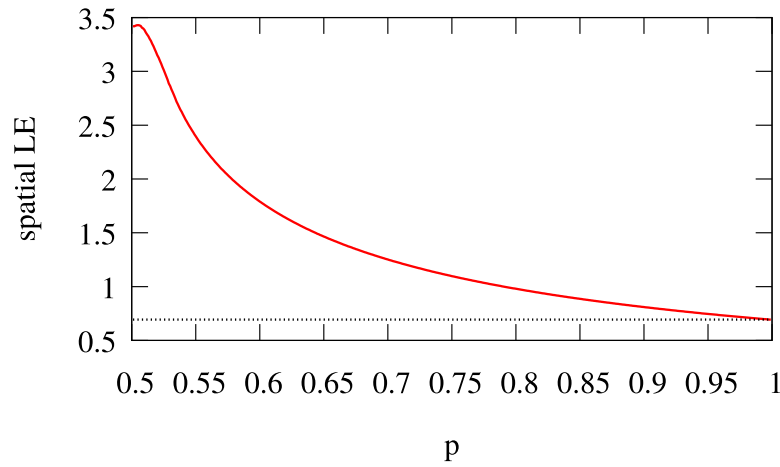


Fig. 11. Spatial Lyapunov exponent λ (Eq. (15)) in dependence on the coupling parameter p . The dotted line is the value $\ln(2)$ to be expected at $p = 1$.

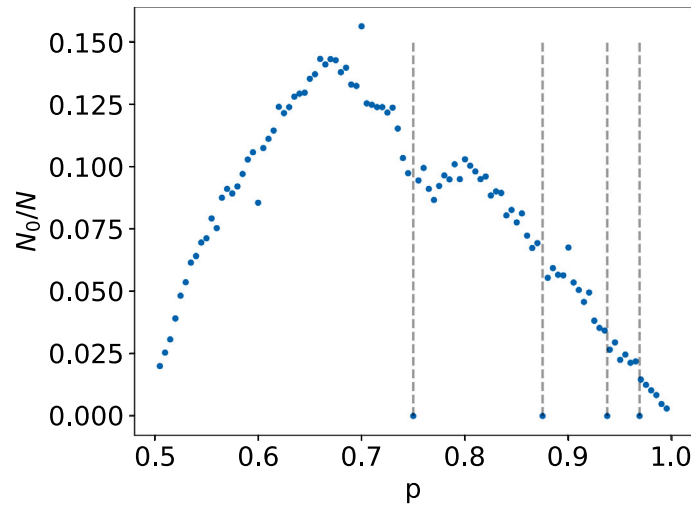


Fig. 12. Fraction of number N_0 that can break the synchronization due a mantissa error over $N = 10000$ randomly extracted in $[0, 1]$ for different values of the coupling parameter p . In dashed line we show the values $\tilde{p} = (2^n - 1)/2^n$.

This difference arises from a combination of computational effects with the convective instability described above.

Here, we argue that in numerical simulations, persistent boundary perturbations can arise, leading, as has been shown in Section 3.3.3, to the loss of synchrony at large distances from the boundary.

Let us consider the *direct coupling* scheme (Eq. (11)), and let t be the time instant at which synchronization between two consecutive nodes

hold: $x_i = x_{i-1}$. In that case, $f(x_i) = f(x_{i-1})$ also holds; however, due to a finite representation of numbers in a digital computer, it is not automatically true that $(1-p)f(x_i) + pf(x_{i-1}) = f(x_{i-1})$, therefore it can happen that $x'_i \neq x'_{i-1}$ (in fact, they differ in computer representation just by one last bit). This can create situations where the states of two consecutive nodes are identical, but the mixing of the factor p and $(1-p)$ desynchronizes them, resulting in $x'_i \neq x'_{i-1}$. This, combined with the

propagation of perturbations, break the stability of synchronized state along the chain.

The effect of a non-exact computation in the direct scheme is state-dependent, it does not happen for all values of x_i . In Fig. 12 we plot the fraction of input x from which a perturbation of the synchronized state can arise due to the finite representation of numbers in the computer. Specifically, the plot shows the number N_0 of values such that $(1-p) * f(x) + p * f(x) \neq f(x)$ out of N random samples of $x \in [0, 1]$ for various values of p . As can be observed, this fraction is non-zero for almost all the considered values of p , showing a maximum around $p \approx 0.67$, before decreasing to zero as $p \rightarrow 1$.

To confirm that this phenomenon is purely artificial and caused by the numerical representation used in the simulation, we note that for certain values (marked by a gray dashed vertical line in figure), the fraction $N_0/N = 0$. These values are $\bar{p} = (2^n - 1)/2^n$ for integer $n > 2$. If we examine the binary representation of these numbers, the effect of multiplying $p' = (1 - \bar{p})$ by $y = f(x)$ is to shift the most significant bit of y by n positions to the right. Since the action of f on x can at most change the first digit from zero to one, the combination of these two effects automatically leads, if $n > 2$, to a fictitious synchronized state. This explains why the complete synchronized state observed in the case of *direct coupling* for $p = 0.75$ in Fig. 8.

Note that the chaotic nature of the local dynamic is crucial: it guarantees that there exists a non-zero probability such that the value of the state x_i is one of the N_0 values that can desynchronize the chain.

In contrast, in the *delta coupling* scheme, this phenomenon does not occur because if $f(x_i) = f(x_{i-1})$, then $p * (f(x_{i-1}) - f(x_i)) = 0$ exactly, and not due to approximations resulting from mantissa error.

4. Conclusions

In our study we explored the synchronization dynamics of a branching chain of unidirectionally coupled chaotic maps, focusing on parent-child and siblings synchronization. This configuration captures the essence of the process on a Cayley tree structure.

We found that both transitions are governed by the corresponding transversal Lyapunov exponents, which can be calculated according to the probability distribution of the driving unit.

We also analyzed the importance of numerical precision in this type of simulations, showing how synchronization windows can depend on machine precision. To support this, we introduced two computational schemes that are mathematically equivalent, but exhibit different behaviors of synchronization across the layers for the deep nodes of the system and large values of the coupling parameter. We have shown that this behavior is caused by a combination of spurious computational effects enhanced by the chaotic local dynamics, amplified along the chain.

We have also shown that, while the re-synchronization dynamics of locally perturbed states is dictated by a velocity-dependent Lyapunov exponent (Eq. (13)), in the case of persistent irregular perturbations it is necessary to introduce the spatial Lyapunov exponent (Eq. (15)).

Remarkably, the two discussed sources of numerical imprecision play different roles: in one case, it leads to a synchronous state although being unstable; in the other case, it breaks synchrony in spite of his stability.

We expect that similar results hold for other maps as well, and also in continuous-time systems, like unidirectionally coupled chains of ordinary differential equations.

CRedit authorship contribution statement

Michele Baia: Writing – review & editing, Writing – original draft, Visualization, Validation, Software, Methodology, Investigation. **Franco Bagnoli:** Writing – review & editing, Writing – original draft, Validation, Supervision, Resources, Methodology, Investigation, Formal analysis, Conceptualization. **Tommaso Matteuzzi:** Writing – review & editing, Validation, Investigation. **Arkady Pikovsky:** Writing – review & editing, Writing – original draft, Visualization, Validation, Supervision, Methodology, Investigation, Formal analysis, Conceptualization.

Declaration of competing interest

The authors declare that they have no known competing financial interests or personal relationships that could have appeared to influence the work reported in this paper.

Data availability

Data will be made available on request.

References

- [1] H. Fujisaka, T. Yamada, Stability theory of synchronized motion in coupled-oscillator systems, *Progr. Theoret. Phys.* 69 (1) (1983) 32–47.
- [2] L.M. Pecora, T.L. Carroll, Synchronization of chaotic systems, *Chaos: An Interdiscip. J. Nonlinear Sci.* 25 (9) (2015) 097611, <http://dx.doi.org/10.1063/1.4917383>.
- [3] D. Febbe, R. Mannella, R. Meucci, A. Di Garbo, Dynamical behaviour of a new model for the UJT relaxation oscillator, *Chaos Solitons Fractals* 183 (2024) 114906.
- [4] K. Li, C. Shi, Synchronization-based topology identification of multilink hypergraphs: a verifiable linear independence, *Nonlinear Dynam.* 112 (4) (2024) 2781–2794.
- [5] K. Li, Y. Lin, J. Wang, Synchronization of multi-directed hypergraphs via adaptive pinning control, *Chaos Solitons Fractals* 184 (2024) 115000.
- [6] S. He, H. Yang, C. Li, X. Shen, Cryptanalyzing an image encryption scheme using synchronization of memristor chaotic systems, *Int. J. Bifurc. Chaos* 34 (11) (2024) 2450138, <http://dx.doi.org/10.1142/S0218127424501384>.
- [7] F. Bagnoli, M. Baia, Synchronization, control and data assimilation of the lorenz system, *Algorithms* 16 (4) (2023) 213, <http://dx.doi.org/10.3390/a16040213>.
- [8] K. Kaneko, Overview of coupled map lattices, *Chaos: An Interdiscip. J. Nonlinear Sci.* (ISSN: 1089-7682) 2 (3) (1992) 279–282, <http://dx.doi.org/10.1063/1.165869>, URL <http://dx.doi.org/10.1063/1.165869>.
- [9] A. Pikovsky, M. Rosenblum, J. Kurths, *Synchronization: A universal concept in nonlinear sciences*, Cambridge University Press, Cambridge, UK, 2003.
- [10] L.M. Pecora, T.L. Carroll, Synchronization in chaotic systems, *Phys. Rev. Lett.* 64 (8) (1990) 821–824, <http://dx.doi.org/10.1103/physrevlett.64.821>.
- [11] T. Wu, X. Zhang, Z. Liu, Understanding the mechanisms of brain functions from the angle of synchronization and complex network, *Front. Phys.* 17 (3) (2022) 31504.
- [12] A.S. Pikovsky, Synchronization and stochastization of the ensemble of auto-generators by external noise, *Radiophys. Quantum Electron.* 27 (5) (1984) 390–395.
- [13] D.S. Goldobin, A. Pikovsky, Synchronization and desynchronization of self-sustained oscillators by common noise, *Phys. Rev. E* 71 (2005) 045201(R).
- [14] F. Flandoli, B. Gess, M. Scheutzw, Synchronization by noise, *Probab. Theory Related Fields* (ISSN: 1432-2064) 168 (3–4) (2016) 511–556, <http://dx.doi.org/10.1007/s00440-016-0716-2>, URL <http://dx.doi.org/10.1007/s00440-016-0716-2>.
- [15] A. Maritan, J.R. Banavar, Chaos, noise, and synchronization, *Phys. Rev. Lett.* 72 (10) (1994) 1451–1454, <http://dx.doi.org/10.1103/physrevlett.72.1451>.
- [16] M.G. Rosenblum, A.S. Pikovsky, J. Kurths, Phase synchronization of chaotic oscillators, *Phys. Rev. Lett.* 76 (11) (1996) 1804–1807, <http://dx.doi.org/10.1103/physrevlett.76.1804>.
- [17] N.F. Rulkov, M.M. Sushchik, L.S. Tsimring, H.D. Abarbanel, Generalized synchronization of chaos in directionally coupled chaotic systems, *Phys. Rev. E* 51 (2) (1995) 980.
- [18] Y. Jiang, P. Parmananda, Synchronization of spatiotemporal chaos in asymmetrically coupled map lattices, *Phys. Rev. E* 57 (4) (1998) 4135–4139, <http://dx.doi.org/10.1103/physreve.57.4135>.
- [19] P. Grassberger, Synchronization of coupled systems with spatiotemporal chaos, *Phys. Rev. E* 59 (3) (1999) R2520–R2522, <http://dx.doi.org/10.1103/physreve.59.r2520>.
- [20] F. Bagnoli, L. Baroni, P. Palmerini, Synchronization and directed percolation in coupled map lattices, *Phys. Rev. E* 59 (1) (1999) 409–416, <http://dx.doi.org/10.1103/physreve.59.409>.
- [21] L. Baroni, R. Livi, A. Torcini, Transition to stochastic synchronization in spatially extended systems, *Phys. Rev. E* 63 (3) (2001) <http://dx.doi.org/10.1103/physreve.63.036226>.
- [22] V. Ahlers, A. Pikovsky, Critical properties of the synchronization transition in space-time chaos, *Phys. Rev. Lett.* 88 (25) (2002) 254101.
- [23] M. Droz, A. Lipowski, Dynamical properties of the synchronization transition, *Phys. Rev. E* 67 (5) (2003) <http://dx.doi.org/10.1103/physreve.67.056204>.
- [24] M. Cosenza, K. Tucci, Pattern formation on trees, *Phys. Rev. E* 64 (2) (2001) 026208.
- [25] A. Singh, S. Jalan, Delay-induced cluster patterns in coupled cayley tree networks, *Eur. Phys. J. Spec. Top.* 222 (3) (2013) 885–893.

- [26] A. Singh, S. Jalan, Heterogeneous delays making parents synchronized: A coupled maps on cayley tree model, *AIP Adv.* 4 (6) (2014).
- [27] P.M. Gade, H.A. Cerdeira, R. Ramaswamy, Coupled maps on trees, *Phys. Rev. E* 52 (3) (1995) 2478.
- [28] F. Bagnoli, M. Baia, T. Matteuzzi, A. Pikovsky, Synchronization of chains of logistic maps, in: *International Conference on Cellular Automata for Research and Industry*, Springer, 2024, pp. 72–84.
- [29] L. Baroni, R. Livi, A. Torcini, Transition to stochastic synchronization in spatially extended systems, *Phys. Rev. E* 63 (2001) 036226, <http://dx.doi.org/10.1103/PhysRevE.63.036226>, URL <https://link.aps.org/doi/10.1103/PhysRevE.63.036226>.
- [30] A. Pikovsky, A. Politi, *Lyapunov exponents: a tool to explore complex dynamics*, Cambridge University Press, Cambridge, UK, 2016.
- [31] A.S. Pikovsky, Comment on “chaos, noise, and synchronization”, *Phys. Rev. Lett.* 73 (21) (1994) 2931.
- [32] I. Aranson, D. Golomb, H. Sompolinsky, Spatial coherence and temporal chaos in macroscopic systems with asymmetrical couplings, *Phys. Rev. Lett.* 68 (24) (1992) 3495.
- [33] A.S. Pikovsky, Local Lyapunov exponents for spatiotemporal chaos, *Chaos: An Interdiscip. J. Nonlinear Sci.* (ISSN: 1054-1500) 3 (2) (1993) 225–232, <http://dx.doi.org/10.1063/1.165987>, arXiv:https://pubs.aip.org/aip/cha/article-pdf/3/2/225/18300069/225_1_online.pdf.
- [34] R.J. Deissler, K. Kaneko, Velocity-dependent Lyapunov exponents as a measure of chaos for open-flow systems, *Phys. Lett. A* 119 (8) (1987) 397–402.
- [35] O. Rudzick, A. Pikovsky, Unidirectionally coupled map lattice as a model for open flow systems, *Phys. Rev. E* 54 (5) (1996) 5107–5115.